Proceedings of the
44th IEEE Conference on Decision and Control, and
the European Control Conference 2005
Seville, Spain, December 12-15, 2005

An Efficient Controller for SV–PWM VSI Based on the Multivariable Structure Function

Eduardo Licéaga-Castro, *Member,* Carlos E. Ugalde-Loo, *Member, IEEE*, Jesús Licéaga-Castro, and Pedro Ponce

***Abstract*—In this paper a novel control strategy for pulse-width modulated voltage source inverters (PWM VSI) is presented. It is based on a linear, diagonal, low order, minimum-phase, fixed, and stable multivariable controller. It is obtained via individual channel design (ICD), a new framework that allows analysis and synthesis of multivariable control systems by means of the multivariable structure function (MSF). Such controller generates the appropriate reference voltage signals for the power inverter via a space-vector PWM (SV-PWM), which in turn provides the voltage signals for the terminals of an induction motor. The theoretical principles behind this control strategy are summarised for completeness. The similarities and differences between some current loop controllers found in literature and the scheme here proposed are discussed. In order to show the ICD controller performance a digital simulation is included. Moreover, it is also shown through the MSF that the dynamical system structure is not sensible to rotor speed or parameter variations. Therefore, it is possible to design a fixed linear robust controller for the whole speed range. Such solution is feasible for engineering applications due to its simplicity and robustness.**

I. Introduction

The control and modelling of AC drives are more complex than those of DC drives. AC machines require converters providing variable-frequency and power supply with the less possible harmonic component. Besides, AC machines are described by rather complex dynamical models subject to parameter variations [5,10,16]. Further difficulties are faced while processing feedback signals with harmonics. To solve this problem, voltage-fed converters are commonly used [1,2]. Such techniques rely on current-controlled PWM converters. Although various current control strategies providing a good performance have been developed in recent years, errors due to transient states, estimation of state variables and ripple due to harmonics are still present [2].

In this paper a novel control strategy for PWM-VSI is presented. It is based on a linear, diagonal, low order, fixed, minimum-phase, and stable multivariable controller. The controller is obtained via individual channel design (ICD), a novel framework that allows analysis and synthesis of multivariable control systems by applying classical techniques based on Bode/Nyquist plots. Such controller generates the appropriate reference voltage signals for the power inverter via a space-vector PWM (SV-PWM), which, in turn, provides the voltage signals for the terminals of an induction motor. Current components represented in a stationary coordinate system are considered. The proposed scheme is robust to variations of the operating conditions and provides free rippled responses and a reduced harmonic content. Good performance is obtained as well.

The paper is organised as follows. A brief description of the SV–PWM VSI is given in Section II. In Section III the motor model is provided. In Section IV the control scheme and a theoretical description of ICD are presented. An analysis of the multivariable structure function associated to the model and robustness issues are fully discussed. Variations in parameters and rotor speed are assessed. In Section V a comparison between current-loop control strategies found in literature and the one here proposed is included. In Section VI some simulations are carried out. Finally, in Section VII the conclusions end the paper.

II. Space Vector Representation of the VSI Output

To describe the inverter output and the analysis of the current control scheme, the concept of space vector (SV) is applied. It gives the possibility to represent three-phase quantities by one space vector [15]. A SV-PWM generates the train of pulses for switching the semiconductors of each line. For instance, let a space vector be defined by

$$\overline{v_s} = (2/3)\left(v_a + a v_b + a^2 v_c\right) \tag{1}$$

where $a = e^{j2\pi/3}$ and $a^2 = e^{j4\pi/3}$. It is considered that the neutrals *N* of the motor and *O* of the DC-link are not connected as in Fig. 1(a). Accordingly, 8 possible conducting modes of the VSI exist. The inverter output voltage, Fig. 1(b), can be represented as [17]:

$$u_k = \begin{cases} (2/3)u_d e^{jk\pi/3} & \text{for } k = 1,\cdots,6 \\ 0 & \text{for } k = 0,7 \end{cases} \tag{2}$$

Each state of switches corresponding to the inverter legs *A, B, C* defines the patterns $S_k = (S_a, S_b, S_c)$, where $S_i = 1$ if the upper switch is conducting while $S_i = 0$ if the lower switch is conducting, with $i = a,b,c$. Each pattern corresponds to one of the vectors u_k (2). For example, if $S_a=1$, $S_b=0$, $S_c=0$, the resulting inverter output voltage vector is $u_1 = (1,0,0)$.

III. Induction Motor Model

The induction motor α–β model is given by [2]:

$$\dot{\omega}_r = (P/2J)(T_E - T_L) \tag{3}$$

$$T_E = \frac{3}{2}\left(\frac{P}{2}\right)\frac{L_m}{L_r}\left(\psi_{\alpha r} i_{\beta s} - \psi_{\beta r} i_{\alpha s}\right) \tag{4}$$

E. Licéaga-Castro is with SEPI-ESIME Ticomán IPN, Ticomán 600, Col. S.J. Ticomán, C.P. 07340, D.F., México (e-mail: eliceagac@uk2.net).

C.E. Ugalde-Loo is with the Department of Electronics and Electrical Eng., Faculty of Engineering, University of Glasgow, G12-8QQ, Glasgow, Scotland, UK (e-mail: kaghlus@hotmail.com).

J. Licéaga-Castro is with the Mechanic and Mechatronics Engineering Department, ITESM-CEM, Carretera Lago de Guadalupe Km.3.5, Atizapán de Zaragoza,C.P.52926,Edo.México,México (e-mail: jliceaga@itesm.mx).

P. Ponce is with the Electrical and Electronics Engineering Department, ITESM-CCM, México (e-mail: pedro.ponce@itesm.mx).

0-7803-9568-9/05/$20.00 ©2005 IEEE

$$
\begin{aligned}
\dot{i}_{\alpha s} &= -\frac{L_r^2 R_s + L_m^2 R_r}{\sigma L_s L_r^2} i_{\alpha s} + \frac{L_m R_r}{\sigma L_s L_r^2} \psi_{\alpha r} + \frac{L_m \omega_r}{\sigma L_s L_r} \psi_{\beta r} + \frac{1}{\sigma L_s} v_{\alpha s} \\
\dot{i}_{\beta s} &= -\frac{L_r^2 R_s + L_m^2 R_r}{\sigma L_s L_r^2} i_{\beta s} - \frac{L_m \omega_r}{\sigma L_s L_r} \psi_{\alpha r} + \frac{L_m R_r}{\sigma L_s L_r^2} \psi_{\beta r} + \frac{1}{\sigma L_s} v_{\beta s} \\
\dot{\psi}_{\alpha r} &= -\frac{R_r}{L_r} \psi_{\alpha r} - \omega_r \psi_{\beta r} + \frac{L_m R_r}{L_r} i_{\alpha s} \\
\dot{\psi}_{\beta r} &= -\frac{R_r}{L_r} \psi_{\beta r} + \omega_r \psi_{\alpha r} + \frac{L_m R_r}{L_r} i_{\beta s}
\end{aligned} \tag{5}
$$

where $i_{\alpha s}$, $i_{\beta s}$ are the stator currents, $\psi_{\alpha r}, \psi_{\beta r}$ are the rotor fluxes, ω_r is the rotor angular velocity, $v_{\alpha s}$, $v_{\beta s}$ are the stator voltages, L_s, L_r, L_m are the stator, rotor, and mutual inductances, R_s, R_r are the stator and rotor resistances, J is the rotor inertia, T_L is the external load torque, P is the number of poles, and $\sigma = 1 - L_m^2/(L_s L_r)$.

Equations in (5) represent the electric dynamics, while (3)-(4) represent the mechanical component of the machine. The inverter control is achieved by controlling system (5).

IV. Induction Motor Model

System (5) can be represented by the state space model

$$
\begin{aligned}
\dot{\mathbf{x}} &= \mathbf{A}\mathbf{x} + \mathbf{B}\mathbf{u} \\
\mathbf{y} &= \mathbf{C}\mathbf{x} + \mathbf{D}\mathbf{u}
\end{aligned} \tag{6}
$$

$$
\mathbf{x} = \left[i_{\alpha s}, i_{\beta s}, \psi_{\alpha r}, \psi_{\beta r} \right]^T \text{ and } \mathbf{u} = \left[v_{\alpha s}, v_{\beta s} \right]^T \tag{7}
$$

$$
\mathbf{A} = \begin{bmatrix} -127.4 & 0 & 90.1 & 8.1\omega_r \\ 0 & -127.4 & -8.1\omega_r & 90.1 \\ 4.97 & 0 & -11.13 & -\omega_r \\ 0 & 4.97 & \omega_r & -11.13 \end{bmatrix}, \mathbf{B} = \begin{bmatrix} 9.15 & 0 \\ 0 & 9.15 \\ 0 & 0 \\ 0 & 0 \end{bmatrix},
$$
$$
\mathbf{C} = \begin{bmatrix} 1 & 0 & 0 & 0 \\ 0 & 1 & 0 & 0 \end{bmatrix}, \mathbf{D} = \begin{bmatrix} 0 & 0 \\ 0 & 0 \end{bmatrix} \tag{8}
$$

where **A**, **B**, **C**, and **D** are the matrices of a typical induction motor [13]. Notice that **A** is stated in terms of ω_r ($\omega_r = 2\pi f_r$). For a particular choice of ω_r, (6) corresponds to a linear system which can be represented in the frequency domain as

$$
\begin{bmatrix} i_{\alpha s}(s) \\ i_{\beta s}(s) \end{bmatrix} = \mathbf{G}(s) \begin{bmatrix} v_{\alpha s}(s) \\ v_{\beta s}(s) \end{bmatrix} \tag{9}
$$

The aim is to design a controller for (6) that provides appropriate references for the SV-PWM VSI, which in turn will supply the voltage signals to the induction motor terminals. Such control is obtained under ICD.

ICD is an analytical framework, with the help of which it is possible to investigate the potential and limitations for feedback design of any multivariable linear time-invariant control system. Although ICD is in principle a feedback structure based on diagonal controllers, it can be applied to any cross coupled multivariable system [6,7]. It is based on the definition of individual transmission channels. In this context the control design is an interactive process that involves the required specifications, plant characteristics, and the multivariable feedback design process itself. Once the channels are defined it is possible to form a feedback loop with the compensator specially designed to meet *customer* specifications. In this manner the multivariable control design problem is reduced to the design of a single-input single-output control for each channel [6].

So far, ICD has been reported in some control strategies, such as in small scale power networks with embedded generation [3], submarines [8], automotive and aerospace industry. With ICD it is possible to reach simple and effective control system design. See for instance [7].

Let a *2*-input *2*-output plant be represented by

$$
\mathbf{Y}(s) = \mathbf{G}(s)\mathbf{u}(s) \tag{10}
$$

$$
\begin{bmatrix} y_1(s) \\ y_2(s) \end{bmatrix} = \begin{bmatrix} g_{11}(s) & g_{12}(s) \\ g_{21}(s) & g_{22}(s) \end{bmatrix} \begin{bmatrix} u_1(s) \\ u_2(s) \end{bmatrix} \tag{11}
$$

where $g_{ij}(s)$ represents scalar transfer functions, $y_i(s)$ the outputs, and $u_i(s)$ the inputs of the system, with $i,j = 1,2$. If a diagonal controller is given by

$$
\mathbf{u}(s) = \mathbf{K}(s)\mathbf{e}(s) \tag{12}
$$

$$
\begin{bmatrix} u_1(s) \\ u_2(s) \end{bmatrix} = \begin{bmatrix} k_{11}(s) & 0 \\ 0 & k_{22}(s) \end{bmatrix} \begin{bmatrix} e_1(s) \\ e_2(s) \end{bmatrix} \tag{13}
$$

with $e_i(s) = r_i(s) - y_i(s)$, where $r_i(s)$ represents the plant references, then the open loop input-output channels are clearly defined from Fig. 2 as

$$
C_i(s) = k_{ii}(s) g_{ii}(s) \left(1 - \gamma(s) h_j(s)\right) \tag{14}
$$

where $i \neq j$ and $i,j = 1,2$. The complex valued function

$$
\gamma(s) = \frac{g_{12}(s) g_{21}(s)}{g_{11}(s) g_{22}(s)} \tag{15}
$$

is referred to as the **multivariable structure function** (MSF). The functions $h_i(s)$ are:

$$
h_i(s) = \frac{k_{ii}(s) g_{ii}(s)}{1 + k_{ii}(s) g_{ii}(s)} \tag{16}
$$

The interaction or cross coupling between the channels can be evaluated through a transfer function, for instance:

$$
d_i(s) = \frac{g_{ij}(s)}{g_{jj}(s)} h_j(s) r_j(s) . \tag{17}
$$

A correct interpretation of (15) is of great importance since

- It determines the dynamical characteristics of each input-output configuration;
- It has an interpretation in the frequency domain;
- Its magnitude quantifies the coupling between channels;
- It is related to the plant transmission zeros;
- $\gamma_a(s)=1$ determines the non-minimum phase condition;
- Its closeness to *(1,0)* in the Nyquist plot indicates to what extent the plant is sensitive to uncertainty in terms of gain and phase margins.

A block diagram of the feedback system with the diagonal controller is shown in Fig. 2(a) and the equivalent scalar channels are shown in Fig. 2(b).

It should be emphasised that in the individual channel representation of the multivariable system there is **no loss of information** [6]. The multivariable character and cross coupling of the plant are contained in the MSF and the cross coupling terms. That is, (14)–(17) are equivalent to:

$$
\mathbf{G}_{\mathrm{cl}}(s) = \left(\mathbf{I} + \mathbf{G}(s)\mathbf{K}(s)\right)^{-1} \mathbf{G}(s)\mathbf{K}(s) \tag{18}
$$

It can be proved that in order to stabilise (18) it is just necessary to stabilise the channels given by (14) [13]. In general stabilisation of the diagonal elements of **G***(s)* is not

required [7]. Moreover, the open loop system dynamical structure with a diagonal controller is summarised in Table I. Notice that the coupling can be expressed in *dB* directly from the channels (14) by means of functions $\gamma(s)h_j(s)$. On the other hand, it is possible to determine the dynamical structure of the system using Table I and analysing the Nyquist plot of $(1-\gamma(s)h_j(s))$.

The dynamical structure of the induction motor is determined by the input-output channels defined by pairing each input to each output. For instance:

(a) $C_1(s)$: $v_{\alpha s}(s) - i_{\alpha s}(s)$ with $\gamma_a(s)=g_{12}(s)g_{21}(s)/g_{11}(s)g_{22}(s)$
$C_2(s)$: $v_{\beta s}(s) - i_{\beta s}(s)$

(b) $C_1(s)$: $v_{\alpha s}(s) - i_{\beta s}(s)$ with $\gamma_b(s)=g_{11}(s)g_{22}(s)/g_{12}(s)g_{21}(s)$
$C_2(s)$: $v_{\beta s}(s) - i_{\alpha s}(s)$

The coupling characteristic of each configuration is determined from $\gamma_a(s)$ and $\gamma_b(s)$ –their associated MSF. Fig. 3 shows $\gamma_a(s)$ structure for different values of ω_r.

The existence and design of stabilising compensators $k_{11}(s)$ and $k_{22}(s)$ can be determined from the characteristics of $\gamma_a(s)$, revealed by its Nyquist/Bode plots shown in Fig. 3. The following analysis was carried out as in [7], where highly coupled and highly sensitive plants were addressed. In this case, the analysis is valid for MSFs corresponding to a rotor frequency within the range of *0.01* to *100 Hz*:

(a.1) The value of $\gamma_a(s)$ as $s \to \infty$ is less than one (in fact is zero), so $1-\lim_{s\to\infty}\gamma_a(s)>0$ and the Nyquist plot of $\gamma_a(s)$ is at the left of the point *(1,0)* for all frequency values.

(a.2) From (15) computed at different values of ω_r, $\gamma_a(s)$ does not contain any RHPP and its Nyquist plot does not encircle the point *(1,0)*. Therefore, using the Nyquist Stability Criterion, $(1-\gamma_a(s))$ does not contain any RHPZ.

(a.3) Due to **(a.1)** and **(a.2)**, $h_i(s)$ do not influence the channel structure at high frequency values. The number of encirclements to *(1,0)* by $\gamma_a(s)h_i(s)$ and $\gamma_a(s)$ coincide.

(a.4) For the analysed control configuration, the transfer functions $g_{ii}(s)$ are minimum phase. Thus, in the product

$$\gamma_a(s)h_i(s)=\frac{g_{ij}(s)g_{ji}(s)}{g_{ii}(s)g_{jj}(s)}\cdot\frac{k_{ii}(s)g_{ii}(s)}{1+k_{ii}(s)g_{ii}(s)}$$

no cancellation of RHPPs of γ_a(s) with RHPZs of $h_i(s)$ occur. Thus, the structure of $(1-\gamma_a(s))$ is preserved by $(1-\gamma_a(s)h_i(s))$ provided that $h_i(s)$ do not have RHPPs. To achieve this, $k_{ii}(s)$ must be designed as a stabilising controller of $g_{ii}(s)$ –not a hard task, since $g_{ii}(s)$ are stable and minimum-phase.

Therefore, the existence of a stabilising controller for channels (14) reduces to the existence of controllers $k_{ii}(s)$ which stabilise simultaneously $g_{ii}(s)(1-\gamma_a(s)h_j(s))$ and $g_{ii}(s)$, with $i,j=1,2\ i\neq j$ (this is the most simple case scenario [7]).

It should be remarked that the definition of stability margins of the channels is possible if their dynamical structure is preserved. That is, $h_i(s)$ should be designed with appropriate stability margins and the Nyquist plot of $\gamma_a(s)h_j(s)$ should not pass near the point *(1,0)*.

It can be concluded that the induction motor model structure has no changes under speed variation (the number of RHPZs and RHPPs is preserved, which in this case are zero). Therefore, it is possible to design a diagonal stabilising controller for (6) for the full range of speed by addressing correctly the characteristics of $\gamma_a(s)$ given before.

The MSF associated with channels in (b) involves a strictly non-proper function for every speed. This indicates that such channel definition is highly coupled. Thus, the design using the paring associated to $\gamma_b(s)$ is avoided.

The following specifications have been considered for the control system design: a bandwidth high enough to track sinusoidal voltage references at *100 Hz*, good stability margins [11], a completely decoupling between the channels, and robustness to parameter variation.

Using the ICD Toolbox reported in [14], the following diagonal controller was obtained

$$k_{11}(s)=k_{22}(s)=\frac{2.1\times10^9\left(s+6\times10^4\right)(s+100)}{s\left(s+1.2\times10^5\right)\left(s+1\times10^5\right)} \qquad (19)$$

Due to the controller characteristics, the design is well suited for engineering applications. The control system performance and robustness measures are presented for the cases of f_r = *60, 10,* and *0.01 Hz* and shown in Figs. 4 to 6.

As stated before, the system structure is not sensible to variations of ω_r. In fact, the coupling between both channels decreases as the speed is decreased. Notice that the coupling at f_r =*0.01 Hz* is negligible. As the structure is preserved under all operating conditions, the controllers (19) have a good performance even at very small frequency values, as shown by the Bode diagrams of the channels in Fig. 4. In fact, the phase and gain margins are high enough to yield a highly robust controller. Notice that the chosen bandwidths are high enough to track sinusoidal inputs at more than *100 Hz*, as it will be addressed in the next section.

Clearly the Nyquist paths of $\gamma_a(s)h_j(s)$ for different ω_r do not pass near the point *(1,0)* and the functions $k_{ii}(s)g_{ii}(s)$ have adequate phase and gain margins, as shown in Figs. 5 and 6. Thus the controller performance and robustness measures can be stated in terms of phase and gain margins. All this information is summarised in Table II.

In Table II, the stability margins associated to functions $\gamma_a(s)h_i(s)$ are summarised. Although one may argue that a gain margin of *8.3 dB* is not high enough to assure robustness, it should be addressed that there are no physical real situations in which the structure of the system is deformed so badly that it passes near *(1,0)*. In fact, under a very critical parameter variation (R_r=*2.5*$R_{r,nom}$,R_s=*2.5*$R_{s,nom}$) $\gamma_a(s)$ structure is still preserved by $\gamma_a(s)h_i(s)$. Therefore, *8.3 dB* is an acceptable gain margin in this particular case. Fig. 7 assesses such variations at f_r = *60 Hz*.

V. Comparison with Other Control Strategies

Due to the great variety of current loop controllers found in literature [1,2,4,5,9,16,17] and the apparent similarity with the proposed scheme (shown in Fig. 8), it is necessary to establish some differences to justify its originality.

In [1,4,5] a scheme consisting of current controllers using three-level hysteresis comparators and a switching table is presented. It involves a variable switching frequency that depends on the load parameters and the AC voltage [1,2,5,9,16]. In certain systems the instantaneous error can increase up to twice the hysteresis band [5]. Also, the use of such controllers adds ripple to the current signals, increasing the harmonic content [2]. A constant switching frequency can be achieved by including a SV–PWM [4,5].

In [5] different control strategies based on PI controllers are addressed, namely the stationary and synchronous PIs. The major problem associated to the stationary PI working in stationary coordinates is a steady-state current error, but it can be solved with a synchronous PI controller [2,5,9]. Nevertheless, such scheme is more complex –it requires two coordinate transformations and the explicit knowledge of the synchronous frequency. There exists an equivalent controller in stationary coordinates, consisting of loops of integrators and multipliers (which form a variable frequency generator that provides voltage references to the PWM stage). A zero steady state error is achieved, but its dynamical performance is worse than that of the stationary PI due to the coupling between α-β components [5]. Also, detuning due to parametric variation is more critical in current controllers working in synchronous coordinates [1].

The synchronous current control with feedforward CEMF compensation is shown in [2]. The scheme uses PI controllers. Compensation is used to eliminate the coupling effect provided by feedback. Such control requires the synchronous frequency and the stator magnetic fluxes.

In [9,10] PI controllers are used. Tuning is achieved by adjusting gains depending on the motor parameters under the assumption that the field is correctly oriented. It is also possible to design the controller by zero-pole cancellation. Nevertheless, the parametric variation may prevent such cancellation, produce an oscillatory or unstable response, or cause field disorientation [2]. In fact, a controller based on plant cancellations is highly sensitive to plant and signal uncertainty and to parameter variation [11,12].

In [1] the use of decoupling networks to achieve an adequate field orientation and control in schemes using synchronous coordinates is suggested. Finally, in [1,5] state feedback linearising controllers are proposed. Nevertheless, the knowledge of the complete state vector and the load torque are required and signal processing is more complex [5,12]. In addition, it is not possible to guarantee robustness under parameter uncertainty or un-modeled dynamics due to plant dynamics cancellation [11,12].

The differences with the proposed scheme are given next:

- The use of PIs is justified as a decoupled plant model is employed (by field orientation or decoupling networks); the ICD controller achieves decoupling without making any special consideration in the plant model or by using any other control structure to guarantee a total decoupling between both channels under any operating condition;
- The ICD controller is highly robust to parameter variation and the dynamical structure of the induction motor is always preserved. Good stability margins are guaranteed under any operating condition. Regardless of the reference frame, a PI controller will not assure robustness to parameter variation by itself;
- The ICD controller allows a sensitivity and disturbance rejection analysis. In addition, the current closed-loop dynamics are linear under any operating condition [13], so the use of a multivariable, diagonal, minimum-phase, stable, robust, and fixed controller is justified.
- Although the proposed scheme works in stationary coordinates, a negligible steady state error is presented.

Because of the previous differences and due to its particular characteristics, the use of the ICD controller poses a new and highly effective control strategy. The control system under ICD is based on the philosophy that decoupling is achieved by the control design. Thus, decoupling networks or special assumptions in the plant model are avoided and an adequate closed-loop performance can be guaranteed. Moreover, a PI or hysteresis controller by itself will never decouple the induction motor model or guarantee robustness, while the ICD controller is able to do both. Therefore, the difference between the proposed strategy and the ones found in literature is clear.

VI. Results

Fig. 9 assesses the performance of the proposed control strategy. The simulation has been carried out under no load conditions and a switching frequency of *20 kHz*. The shown results are adequate: the controller provides perfect tracking under frequency, amplitude, and parameter variation.

The total harmonic distortion of the current waveforms is negligible ($THD_{i\alpha s}= THD_{i\beta s}=0.3\%$) as well as the error both in stationary and synchronous coordinates.

It should be emphasised that the employment of a robust controller for the SV-PWM VSI (as yielded by the ICD approach) is the first step towards the achievement of a successful, simple, and efficient controller for a typical induction motor [13]. Its closed–loop characteristics can be fully exploited while estimating the unit vector –the key issue in Field Oriented Control. Furthermore the speed control can be simplified to a straightforward design [13].

VII. Conclusion

A space vector pulse width modulated individual channel design controller for voltage source inverters is presented. Its features are: robust, fixed, low order, linear, diagonal, stable, and minimum-phase. Its robustness assessment is possible due to the nature of the design procedure followed. The advantages of the proposed scheme are: the possibility of tracking current references under frequency, amplitude, and parametric variation, and current waveforms with negligible total harmonic distortion and mean square error. In addition the SV-PWM with a carrier signal has certain advantages over traditional methods. Moreover, its implementation is straightforward and does not require any

tables. These facts render a well suited design for engineering applications.

REFERENCES

[1] I.Boldea,S.A.Nasar. *Vector control of AC drives.* USA: CRC, 1992.

[2] B.K. Bose. *Power electronics and variable frequency drives.* USA: IEEE Press, 1993.

[3] G.J.W. Dudgeon, W.E. Leithead, J. O'Reilly, and J.R. McDonald "Prospects for the decentralized control of small-scale power networks with embedded generation" *IEEE Power Engineering Society Summer Meeting*, no 2, pp 1399-1404, 2000.

[4] M.P. Kazmierkowski, M.A. Dzieniakowski, W. Sulkowski, "Novel space vector based current controllers for PWM-Inverters," *IEEE Trans. on Power Electronics*, vol. 6, no 1, pp 158-166, Jan. 1991.

[5] M.P. Kazmierkowski, R. Krishnan, and F. Blaabjerg. *Control in Power Electronics. Selected Problems.* USA: Academic Press, 2002.

[6] W.E. Leithead, J. O'Reilly, "M-input m-output feedback control by ICD," *International Journal of Control*, 56, pp 1347-1397, 1992.

[7] E.Licéaga, J.Licéaga, C.Ugalde, "Beyond the existence of diagonal controllers: from the relative gain array to the multivariable structure function" To be presented at: *44th IEEE CDC-ECC,* Spain, 2005.

[8] E. Licéaga, J. Licéaga, "Submarine depth control by individual channel design," *Proc.37th IEEE CDC*, 3, pp. 3183–3188, 1998.

[9] N. Mohan. *Advanced Electric Drives: Analysis, Control and Modeling using Simulink*. USA: Mnpere, 2001.

[10] Mohan.*Electric drives–An integrative approach.*USA:Mnpere,2001.

[11] S. Skogestad, and I. Postlethwaite. *Multivariable feedback control. Analysis and design.* UK: John Wiley & Sons, 1996.

[12] J.J.E.Slotine,W.Li.*Applied nonlinear control.*USA:PrenticeHall,1991.

[13] C.Ugalde. *Control de motores de inducción utilizando la función de estructura multivariable.* MSc.Dissertation. IPN SEPI ESIME, 2005.

[14] C.E.Ugalde-Loo, E.Licéaga-Castro, J.Licéaga-Castro, "2x2 Individual Channel Design MATLAB® Toolbox". To be presented at: *44th IEEE CDC-ECC,* Spain, 2005.

[15] H.W. van der Broeck, H.C. Skudelny, and G.V. Stanke, "Analysis and Realization of a Pulsewidth Modulator Based on Voltage Space Vectors," *IEEE Tran.Ind.App.*,vol.24,no.1,pp.142–150, Jan/Feb.1988.

[16] P.Vas.*Sensorless vector and direct torque control.*USA:Oxford,1998.

[17] P.Vas. *Vector control of AC machines.* USA: Oxford, 1990.

Table I. *Dynamical structure of open loop channels*

Channel	Zeros	Poles
$C_1(s)$	Zeros of $(1-\gamma(s)h_2(s))$	Poles of $g_{11}(s)$, $g_{12}(s)$, $g_{21}(s)$, $h_2(s)$
$C_2(s)$	Zeros of $(1-\gamma(s)h_2(s))$	Poles of $g_{22}(s)$, $g_{12}(s)$, $g_{21}(s)$, $h_1(s)$

Table II. *Control system structural robustness assessment*

Measure	C_1	$K_{11}g_{11}$	$\gamma_a h_2$	C_2	$K_{22}g_{22}$	$\gamma_a h_1$
BW[rad/s]	$1x10^5$	$1x10^5$	—	$1x10^5$	$1x10^5$	—
G_M [dB]	∞	∞	8.3	∞	∞	8.3
P_M [deg]	64	64	∞	64	64	∞

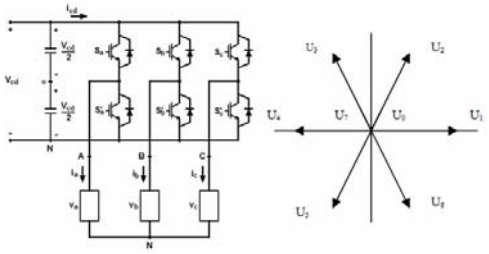

(a) *(b)*

Fig. 1. *(a) Simplified diagram of a VSI feeding an induction motor; (b) Space vector representation of output voltage*

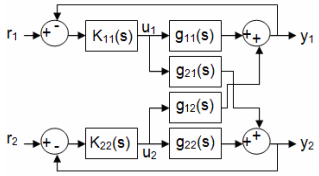

Fig. 2. *(a) 2-input 2-output system with a diagonal controller*

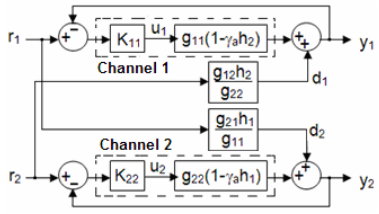

Fig. 2. *(b) Equivalent channel representation*

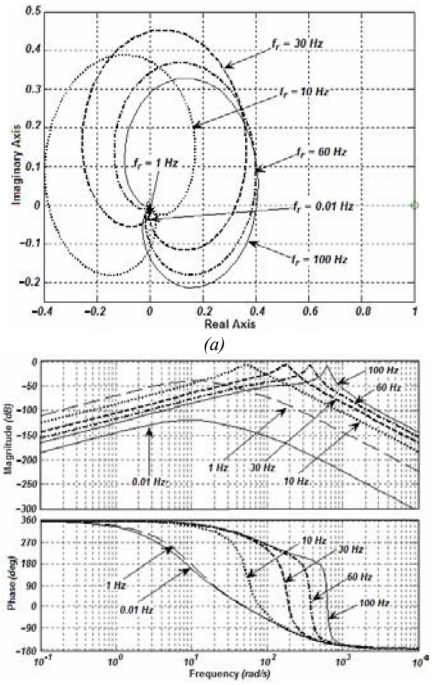

(a)

(b)

Fig. 3. *Assessing $\gamma_a(s)$ structure for different ω_r ($\omega_r=2\pi f_r$): (a) Nyquist plot; (b) Bode plot*

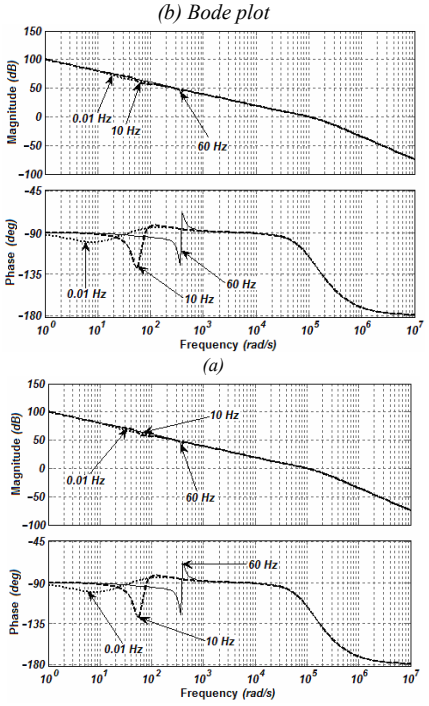

(a)

(b)

Fig. 4. *Assessing controller performance at different ω_r. Bode plot: (a) Channel 1; (b) Channel 2*

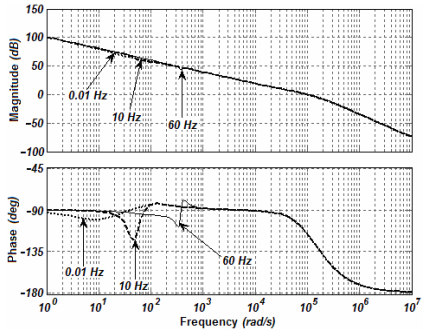

(a)

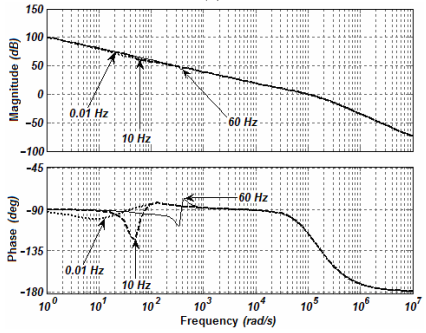

(b)

Fig. 5. *Structural robustness assessment. Bode plot: (a) $k_{11}g_{11}$; (b) $k_{22}g_{22}$*

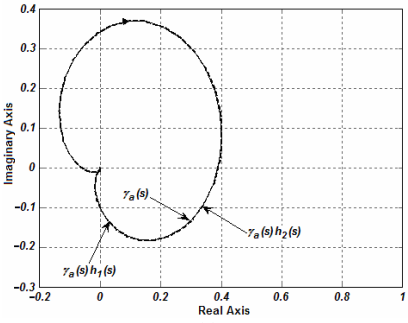

(a)

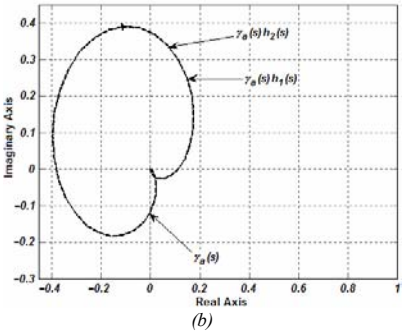

(b)

Fig. 6. *Channel 1 & 2 structural robustness assessment. Nyquist diagrams of γ_a vs $\gamma_a h_2$ vs $\gamma_a h_1$ at (a) 60Hz; (b) 10Hz*

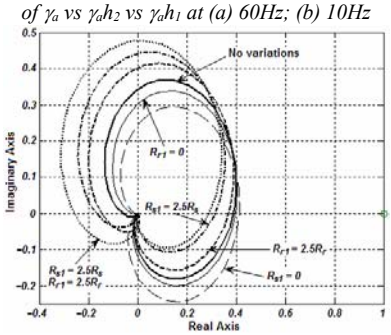

Fig. 7. *Structural robustness assessment. Nyquist diagram of γ_a at f_r = 60Hz under parameter variation.*

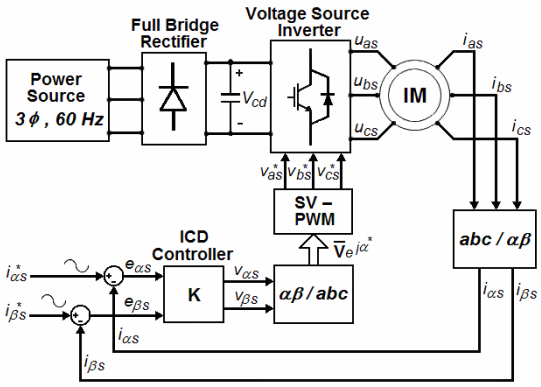

Fig. 8. *Block diagram of proposed control scheme strategy for the VSI*

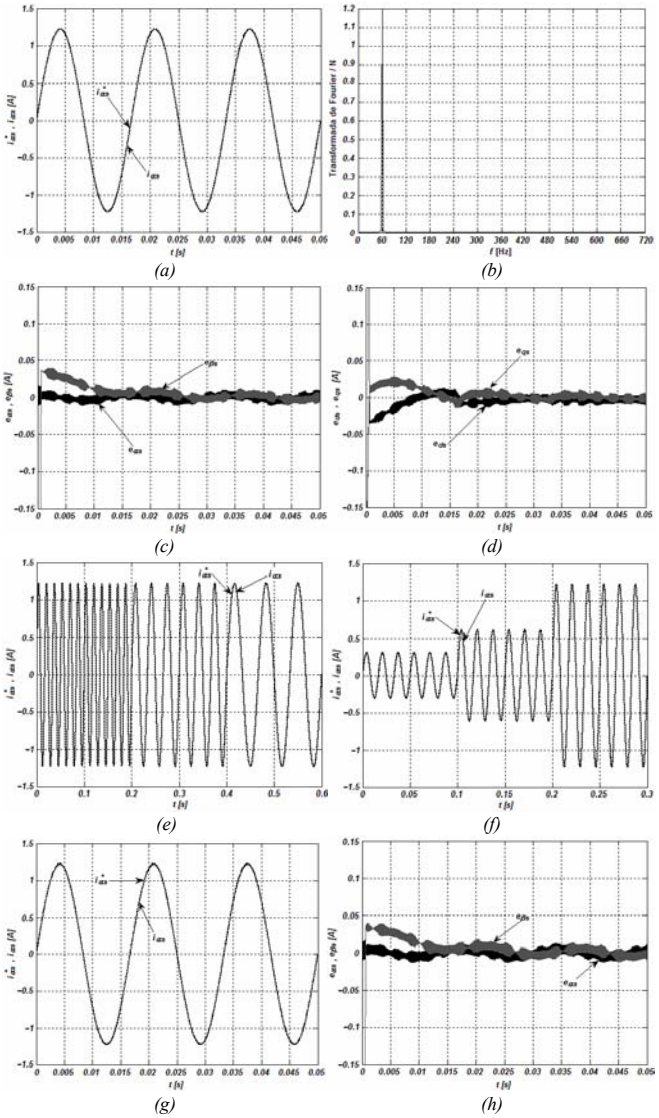

(a) (b) (c) (d) (e) (f) (g) (h)

Fig. 9. *ICD controller performance: (a) Reference vs α-axis current; harmonic components of α-axis current; (c) current error in stationary coordinates; (d) current error in synchronous coordinates; (e) frequency variation; (f) amplitude variation; (g) reference vs α-axis current under parameter variation (250% in R_s and R_r); (h) current error under parameter variation*